Morphological-evolution pathway during phase separation in polymer solutions with highly asymmetrical miscibility gap

Gang Zhang, Tao Yang, Sen Yang, and Yunzhi Wang

Phys. Rev. E **96**, 032501 — Published 11 September 2017

DOI: 10.1103/PhysRevE.96.032501

Morphological evolution pathway during phase separation in polymer solutions with highly asymmetrical miscibility gap

Gang Zhang[a,b], Tao Yang[a,*], Sen Yang[b], Yunzhi Wang[a,c,*]

[a] Center of Microstructure Science, Frontier Institute of Science and Technology, State Key Laboratory for Mechanical Behavior of Materials, Xi'an Jiaotong University, Xi'an 710049, China

[b] MOE Key Laboratory for Nonequilibrium Synthesis and Modulation of Condensed Matter, School of Science, Xi'an Jiaotong University, Xi'an 710049, China

[c] Department of Materials Science and Engineering, The Ohio State University, Columbus, OH 43210, USA

ABSTRACT

Microstructural evolution during thermally-induced phase separation in a polymer solution with a highly asymmetrical miscibility gap is analyzed using Flory-Huggins thermodynamics and non-linear Cahn-Hilliard kinetics. Computer simulation results demonstrate that, in contrast to systems with symmetric miscibility gaps, new morphological evolution pathways (MEPs) including cluster-to-percolation (CTP) and percolation-to-cluster (PTC) transitions are identified. These MEPs are rationalized according to asynchronous evolution of the two product phases. For a highly asymmetric polymer system, the initial solution composition is also found to play a critical role in determining the MEPs. According to the simulation results a map of MEPs in terms of initial solution composition and aging time of phase separation is established to guide future microstructural design in asymmetrical polymer solutions.

1. INTRODUCTION

Owing to the advantage of producing narrow pore size distribution and the easiness of processing, thermally-induced phase separation (TIPS) in polymer solutions has been used widely in synthesizing porous polymeric membranes, foams, and gels [1–6]. To date, considerable attentions have been given to the mechanisms underlying the formation of various distinctively different morphological patterns of the two-phase mixture during TIPS and the roles played by some of the core factors such as polymer concentration, quench depth and cooling rate [7–10]. Nevertheless, little study has been conducted on the difference in molecular weight (MW) or degree of polymerization (DP) of the co-existing phases in polymer solutions, especially its influence on morphological evolution. Experimentally, Matsuyama et al. [11] reported that as the MW of polypropylene decreased, the cloud point curve shifted to a lower temperature region and the morphology of the membrane changed from an interconnected structure to a cellular pore structure. However, the microstructural evolution during the early and intermediate stages of TIPS was not provided, which is critical to understand the formation of the final microstructure. In addition, the volume fraction of polymer was fixed and the influence of initial composition of the polymer solution on microstructure development was not studied. More recently, the effect of PVDF molecular weight on hollow fiber membranes synthesized by the TIPS technique was investigated [12]. However, only final morphologies formed at different MWs were shown and the morphological evolution process is lacking, which is important for precisely controlling the microstructure and properties of membranes.

Employing a numerical model of dissipative particle dynamics, Wang *et al.* [13,14] studied the effect of polymer MW (polymer chain length) on membrane formation, with a focus on the *kinetic* aspect and little attention on morphological evolution. In addition, this kind of particle-level model is limited to small number of particles and short time scales.

For spinodal decomposition in metals and ceramics, it has been taken for granted that a percolated (or interconnected) microstructure forms for a critical quench while cluster-like (or droplet-like) pattern develops for an off-critical quench. This is also true for polymer blends where the MWs of components are all large and, thus, the miscibility gaps are symmetric or nearly symmetric. In contrast to metallic and ceramic materials as well as polymer blends, however, polymer solutions consist of at least two types of molecules with significantly different MW or DP, e.g., a polymer and its solvent, leading to strongly asymmetrical miscibility gaps [15]. Thus the knowledge developed based on spinodal decomposition in polymer blends (or metallic and ceramic systems) may break down when highly asymmetrical miscibility gaps are encountered in polymer solutions. The morphological evolution pathways (MEPs) during spinodal decomposition in systems having highly asymmetrical miscibility gaps could deviate significantly from those found in systems with symmetrical miscibility gaps, leading to drastically different microstructural patterns. Therefore, it is of great theoretical and technological significance to study systematically microstructural evolution during spinodal decomposition in a system having a highly asymmetrical miscibility gap in contrast to that in a system having a

symmetrical miscibility gap. This will allow us to develop fundamental understanding of the differences in terms of the microstructural evolution sequence in the two cases and making use of it to design novel polymeric membrane microstructures with unprecedented properties. So far, several experiments on morphological development in polymer solutions undergoing TIPS were reported [16–18]. However, little work on the MEPs at various polymer concentrations for a highly asymmetric polymer solution is carried out. On the other hand, many modeling works on the morphological evolution in polymer-solvent systems have been conducted using the Flory-Huggins (FH) theory [19–23], but most of the systems considered have rather low DP polymers (e.g., the DP is much less than 100) and thus less asymmetrical miscibility gaps because a high DP gives rise to numerical instability using the FH free energy model in simulations. Chan et al. [20,23] used the Galerkin finite element method to simulate microstructure evolution for polymer-solvent systems with asymmetrical miscibility gaps, but the value of DP considered is ~ 10. Using a molecular modeling, Termonia [24] also studied microstructural developments upon quenching in a polymer solution with a large DP of polymer. However, their attention was focused on the initial stage of the spinodal decomposition and only an off-critical composition was considered.

In this study, microstructural evolution in a binary polymer-solvent system with a highly asymmetric miscibility gap and an upper critical solution temperature (UCST) is investigated numerically by using the Flory-Huggins theory for thermodynamics and nonlinear Cahn-Hilliard theory for kinetics. The thermodynamic parameters used

in the simulations are derived from the PMMA/cyclohexanol system and, thus, the DP of polymer in our simulations is chosen to be 100, which is close to the DP value of PMMA [25]. In order to bypass the numerical instability of the FH free energy model in a highly asymmetrical system, a polynomial free energy form fitted to the FH model is used. Various initial solution compositions including both critical and off-critical cases are considered in the simulations. The entire phase separation processes are documented and a MEP map is constructed to guide future microstructure design of polymeric membranes by TIPS.

2. THEORETICAL MODEL AND NUMERICAL METHOD

In the present study, we consider an incompressible polymer solution consisting of solvent A and polymer B with an UCST-type phase diagram, which has a well-defined free energy functional according to the gradient thermodynamics [26,27]:

$$F\{c(\mathbf{r})\} = \int_V \left[f(c) + \kappa(\nabla c)^2 \right] d\mathbf{r} \tag{1}$$

where c is the concentration of solvent A, V is the total volume of the system and κ is the gradient energy coefficient characterizing contributions from concentration non-uniformity to the total free energy. The first term in the integrand is the local free energy density and can be approximated by the classical Flory-Huggins (FH) lattice theory [28–30]:

$$f(c)=\frac{k_{\mathrm{B}}T}{v_0}\left[\frac{c}{N_{\mathrm{A}}}\ln c+\frac{1-c}{N_{\mathrm{B}}}\ln(1-c)+\chi c(1-c)\right] \tag{2}$$

where k_{B} is the Boltzmann constant, T is temperature, v_0 is the volume of a polymer monomer (assumed to be same as the volume of a solvent molecule), χ is the FH interaction parameter, N_{A} and N_{B} denote the DP of solvent A and polymer B, respectively.

Since the present study focuses mainly on the effect of asymmetry of the miscibility gap on morphological pattern formation during the spinodal decomposition, the hydrodynamic effect is neglected. Under this condition, the kinetics of the phase separation can be described by the nonlinear Cahn-Hilliard (CH) diffusion equation [31,32]:

$$\frac{\partial c(\mathbf{r},t)}{\partial t}=\nabla\cdot M(t)\nabla\frac{\delta F}{\delta c(\mathbf{r},t)}+\xi(\mathbf{r},t) \tag{3}$$

where $M(t)$ is the chemical mobility and is assumed to be a constant in this study, ξ is the Gaussian stochastic field representing the effect of thermal noise, which obeys the fluctuation-dissipation theorem [33]:

$$\left\langle \xi(\mathbf{r},t)\xi(\mathbf{r}',t')\right\rangle=-2k_{\mathrm{B}}TM\nabla^2\delta(\mathbf{r}-\mathbf{r}')\delta(t-t') \tag{4}$$

By using the following scaling relations: $c^*=c$, $t^*=2M\kappa t/L^4$, $x^*=x/L$, $y^*=y/L$, $z^*=z/L$, $T^*=T/T_{\mathrm{c}}$ and $D^*=k_{\mathrm{B}}T_{\mathrm{c}}L^2/(2\kappa v_0)$, where T_{c} corresponds to the critical temperature, and L is the length of the simulation cell, a dimensionless governing equation can be written as:

$$\frac{\partial c^*}{\partial t^*} = \nabla^{*2}\left\{ D^* T^* \times \left[\frac{1}{N_A} + \frac{1}{N_A} \ln c^* - \frac{1}{N_B} - \frac{1}{N_B} \ln(1-c^*) + \chi\left(1-2c^*\right) \right] - \nabla^{*2} c^* \right\} + \xi^*\left(\mathbf{r}^*, t^*\right) \tag{5}$$

where the superscripted asterisks denote dimensionless quantities. In this study, a binary polymer solution system comprised of small molecule solvent A and polymer B with UCST is considered and the FH interaction parameter χ is temperature-dependent and has the form of $\chi = -5.068 + 1900.6/T$ [25]. The DPs of the solvent and polymer are chosen as $N_A = 1$ and $N_B = 100$, respectively.

Equation (5) is solved numerically by using a second-order central difference method in real space and the Adams predictor-corrector scheme in time for a higher stability. The initial conditions are described by $c^*\left(\mathbf{r}^*, t^* = 0\right) = c_0^* + \delta c^*$, where c_0^* is the average solution composition and δc^* represents infinitesimal random fluctuation. The initial state is obtained by averaging several independent simulation runs with different random numbers. A periodic boundary condition is imposed in each direction. The dimensionless sizes of simulation domains are set to be 256×256 in 2D and 128×128×128 in 3D. For simplicity, the superscripted asterisks of the dimensionless parameters are neglected in the following sections.

3. SIMULATED RESULTS

In this study, all simulations are performed at the quench temperature $T^* = 0.95$ and the corresponding free energy density curve calculated according to the FH free energy model is shown in Fig. 1 by the blue curve. However, the numerical instability

arises from the logarithm term in the FH free energy model when the concentration approaches to 0 or 1. In order to circumvent this problem, a fitted polynomial function is adopted to replace the FH free energy density in the simulations, which is also presented in Fig. 1 by the red curve. Besides, the binodal, spinodal, and critical points calculated using the fitted polynomial function are marked in the polynomial free energy density curve, i.e., B1, B2, S1, S2, and C. The concentrations corresponding to B1, S1, C, S2, B2 points are 0.3790, 0.5288, 0.8457, 0.9276, and 0.9999. Moreover, the points from I to V represent the solution compositions investigated to reveal various MEPs. The concentrations corresponding to I, II, III, IV, and V are 0.58, 0.6895, 0.74, 0.79, 0.92, respectively.

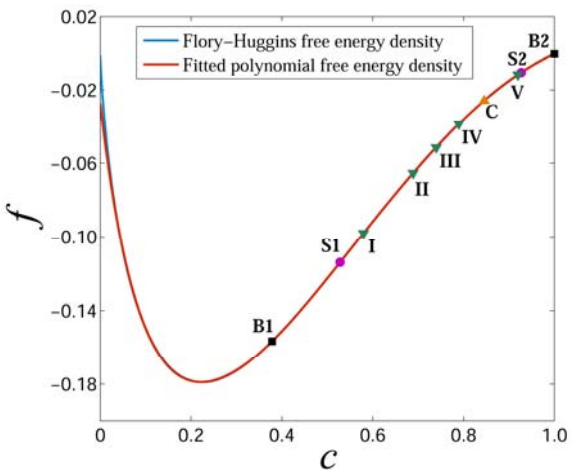

FIG. 1. Free energy density curves obtained by the FH model (blue color) and the fitted polynomial (red color). B1, B2, S1, S1, C represent binodal, spinodal, and critical concentrations; I, II, III, IV, V are the characteristic compositions used to determine various MEPs.

For comparison, two solutions with typical off-critical (at point II in Fig. 1) and critical (at point C in Fig. 1) compositions are first investigated. The dimensionless parameters used in the simulations are: $D = 1.17$, $dt = 0.01$, $dx = dy = 1$. The temporal

evolution of the microstructure is shown in Fig. 2 for former and in Fig. 3 in the latter, where the blue and red regions represent polymer-rich (α) and solvent-rich (β) phases, respectively. It can be seen from Fig. 2(a) that more or less equiaxed and discrete β droplets form first at t = 150. Then both the β droplets and α matrix evolve towards their equilibrium compositions, leading to a well-separated two-phase pattern at t = 180 (Fig. 2(b)). In the meantime, some β droplets start to coalescence with their neighbors and become interconnected (see the rectangles at the upper-left corners of the simulated images in Fig. 2). Eventually, sausage-shaped β droplets (still discrete) embedded in a continuous α matrix is formed at t = 500 (Fig. 2(d)) and both phases have reached their equilibrium compositions and volume fractions (i.e., 50:50 for composition point II). In this decomposition process, the two-phase microstructure has experienced a morphological transition from equiaxed solvent (β, red in color) droplets embedded in a continuous polymer matrix to sausage-shaped solvent droplets embedded in a continuous polymer matrix. This phenomenon can be named as a "cluster-to-percolation" (CTP) transition and has been observed directly in the experiments where the polymerization/curing reaction is coupled to a phase separation process [34,35].

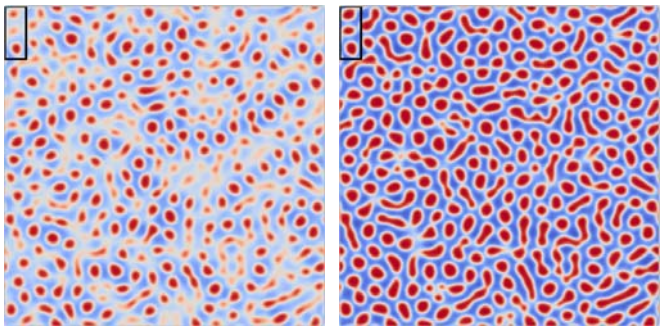

(a) (b)

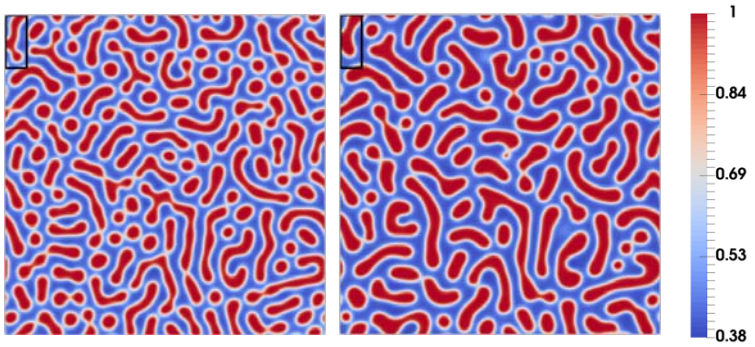

(c) (d)

FIG. 2. Temporal evolution of microstructures for an off-critical quench with initial composition c_0 = 0.6895. (a)–(d) correspond to the reduced times: t = 150, 180, 320, and 500.

At the critical point C with composition c_0 = 0.8457 (Fig. 3), a more or less percolated two-phase microstructure emerges at the early stages of decomposition (Fig. 3(a)), with a few equiaxed α droplets. Then the percolated microstructure evolves gradually into discrete and equiaxed α droplets embedded in a continuous β matrix (Fig. 3(d)). The break-up of the initially interconnected polymer-rich α phase into discrete polymer droplets can be readily seen in the region highlighted by the rectangles in the simulated images obtained at different times. In this case, the system has experienced a morphological transition from a more or less percolated two-phase microstructure to one with equiaxed polymer-rich droplets embedded in a continuous solvent-rich matrix. This phenomenon can be referred to as a "percolation-to-cluster" (PTC) transition in order to parallel to the term CTP above. This PTC transition is different with the PTC phenomenon mentioned in literatures [24,36–43], which will be discussed in the later section of this paper.

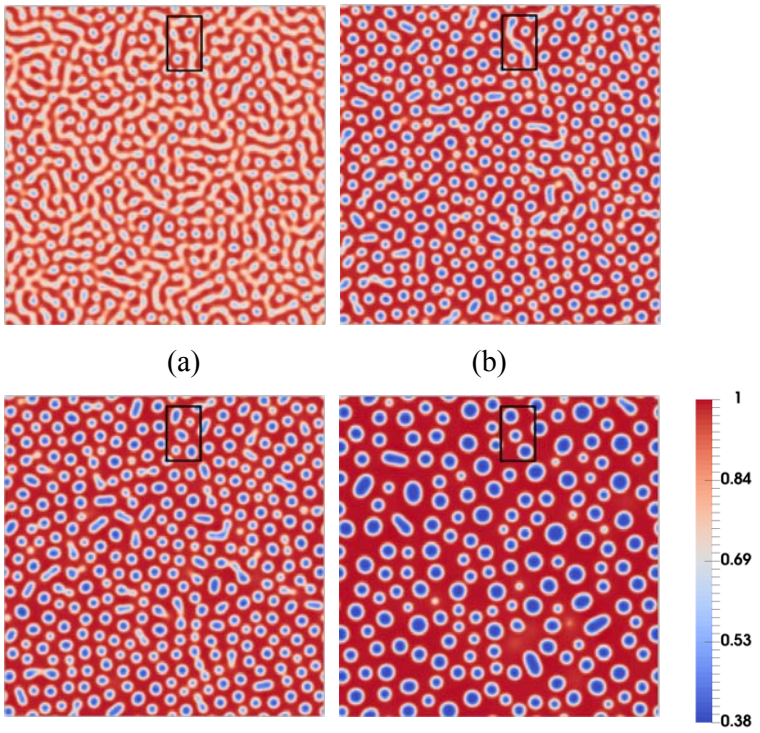

FIG. 3. Temporal development of microstructure for the critical quench with initial composition c_0 = 0.8457. (a)–(d) correspond to the reduced times: t = 50, 106, 140, and 500.

The three-dimensional (3D) simulations revealing the temporal evolution of microstructure for the point II in Fig. 1 with c_0 = 0.6895 and point C with c_0 = 0.8457 are shown in Fig. 4. As can be readily seen, the characteritics of CTP and PTC transitions are also clearly observed in Figs. 4(a)–4(c) and Figs. 4(d)–4(f), which are consistent with the 2D simulation results. In order to exhibit the 3D structure more clearly, the yellow color in each image is adopted and represents the iso-concentration contour surface, and the contour value is the average of maximum and minimum of concentration fluctuation. This 3D simulation indicates that the CTP and PTC phenomena are independent of the dimensionality and are universal characteristics for the polymer system with a highly asymmetric miscibility gap.

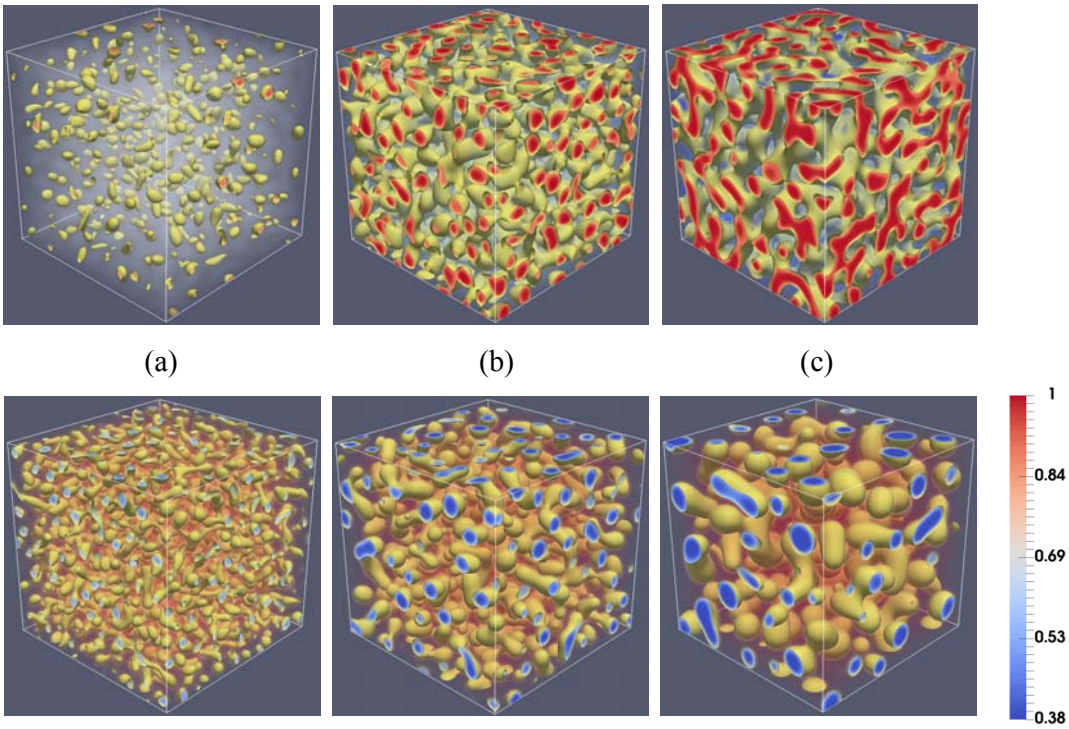

FIG. 4. Microstructural evolution of the CTP and PTC transitions in 3D space: (a–c) for initial composition c_0 = 0.6895 with reduced time: t = 150, 180, and 320; (d–f) for initial composition c_0 = 0.8457 with reduced time: t = 75, 250, and 750. The yellow color in each image represents the iso-concentration contour surfaces.

4. DISCUSSION

4.1. Asynchrony in concentration wave development and its effect on microstructure

Usually for spinodal decomposition in systems having a symmetrical miscibility gap a cluster-like microstructure forms at a composition far off the critical composition or a percolated microstructure forms at or near the critical composition in the early stages and the characteristics of the microstructures maintain during the subsequent evolution. However, for a polymer solution with a highly asymmetric miscibility gap considered in this study, distinctly different cluster-to-percolation

(CTP) and percolation-to-cluster (PTC) transitions are observed, as shown in Figs. 2 and 3, respectively. In order to understand the differences in microstructure development in the asymmetric and symmetric systems, below we analyze concentration variation, diffusion flux and microstructural evolution pathway (MEP) in the two cases.

Figure 5(a) shows the time-evolution of concentrations in the α (blue) and β (red) phase regions for entire sample and local concentration at point *a* in Fig. 5(b) that is part of the microstructures shown in Fig. 2 marked by the black rectangle in the upper-left corner. In Fig. 5(a) the red and blue curves are for concentrations in the β and α phases, respectively and the green curve is for concentration at point *a*. The temporal evolutions of the microstructure and the diffusional fluxes are presented in Figs. 5(b)–5(d). The black solid lines in Fig. 5(a) are tangent to each part of the concentration curve and the magnitudes of their slopes are utilized to evaluate the growth rate of each phase during the early stages of decomposition. In accordance with the time characteristic of structure factor curve, the time period in the solid line region corresponds to the early stage of phase separation [44,45].

It is remarkable that the tangent slope of the red curve is much larger than that of the blue curve during the same time period, indicating the growth rate of the β phase (solvent-rich, represented by the red color) is much greater than that of the α phase during the early stage of spinodal decomposition. From Fig. 5(a) we can see that the β phase has reached its equilibrium composition (but not the equilibrium volume fraction yet) at t = 150 while the α phase composition is still far from equilibrium at

this moment. Consequently, the bulk thermodynamic driving force for the concentration change in the β phase regions has diminished while the concentration evolution in the α phase regions continues. This asynchrony in growth can also be seen in Figs. 5(c) and 5(d), where vanishing flux gradients are observed in the dark red-colored regions while finite flux gradients are present in the blue-colored regions, directing from the deep blue (polymer-richer) regions to the light blue (less polymer-rich) area (see point *a* in Fig. 5(b) and areas enclosed by the white boxes in 5(c) and 5(d)). This causes a secondary phase separation in the α matrix, with the solvent concentration in the gaps between adjacent β phase regions continues to growth, depleting solvent from the surrounding polymer-rich α phase regions. As time proceeds, the gaps gradually transform from α phase into β phase until the α phase reaches its equilibrium composition and volume fraction, causing the coalescence of the adjacent β phase droplets and thus the 'cluster-to-percolation' (CTP) morphological transition as exhibited in Fig. 2. Note that the Gibbs-Thompson effect for domain coarsening also played a role in this coalescence process. The time-evolution of the concentration at point *a* in Fig. 5(b) is shown in Fig. 5(a) by the green colored curve. It first decreases toward the solvent-lean α phase and then increases back toward the solvent-rich β phase.

Thus, the much faster rate for the solvent-rich β phase domains to reach the equilibrium concentration (but with the volume fraction of the β phase far below the equilibrium value of 50%) as compared to that of the polymer-rich α phase may have led to an β cluster structure in a continuous α matrix at the early stages of

decomposition (e.g., at t = 150, as shown in Fig. 2(a)) and the subsequent CTP transition at latter stages when both the concentration and volume fraction of the two phases reach equilibrium. Note that the final microstructure is neither an ideal cluster-like structure nor a perfect percolated structure as shown in Fig. 2(d).

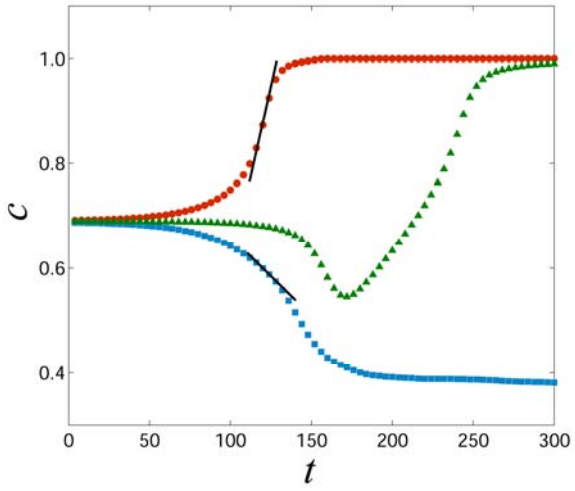

(a)

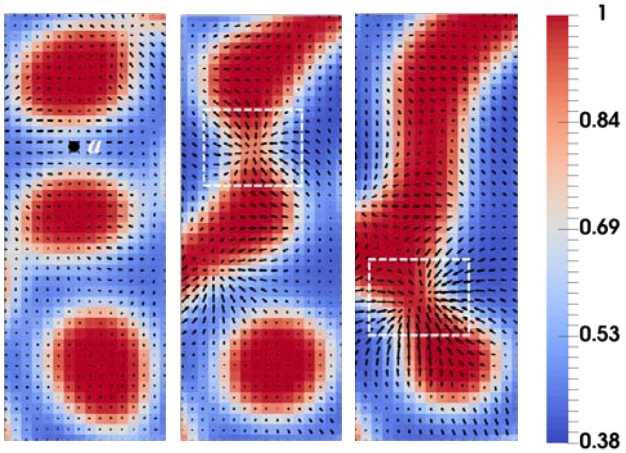

(b) (c) (d)

FIG. 5. (a) Concentration change curves of β (red) and α (blue) phases and point *a* (green) in (b) for the solution of composition c_0 = 0.6895; (b–d) temporal evolution of local microstructure and diffusional fluxes at reduced times: t = 180, 240, and 320.

The time-evolution of concentrations in the α and β phases for the entire sample and at point *b* in Fig. 6(b) are shown in Fig. 6(a), where the red and blue curves are

for concentrations in the β and α phases, respectively and the green curve is for concentration at point *b*. The temporal evolutions of the microstructure and the diffusional fluxes are shown in Figs. 6(b)–6(d). By comparing the tangent slopes of the concentration curves of the two product phases during the early stages, it is found that the growth rate of the α phase is just slightly greater than that of the β phase. But because of the difference in deviations of the equilibrium compositions of the two phases from the starting solution composition, the β phase has arrived at its equilibrium composition at $t \sim 50$ while the α phase is still far away from its equilibrium composition. Therefore, the concentration in the α phase regions continues to evolve. In Figs. 6(b) and 6(c), a vanishing flux gradient is observed in the dark red-colored regions while a finite flux gradient is present in the blue-colored regions, directing from the dark blue-colored to light blue-colored areas (see the enclosed regions by the white boxes). This leads to a secondary decomposition of the α phase (blue) regions, with the light blue regions gradually evolving into red (β phase) regions until the equilibrium condition is achieved, leading to the 'percolation-to-cluster' (PTC) morphological transition as shown in Fig. 3. The time-evolution of the local concentration at point *b* first decreases toward that of the α phase and then increases back toward to that of the β phase, indicating that the percolated α phase regions break up and form a cluster-like structure. In this case, the two product phases also asynchronously arrive to their equilibriums by a two-step decomposition process, resulting in the PTC transition. Note that the final cluster-like structure is similar to the cluster-like structure formed at the off-critical composition

in a symmetric polymer system. Therefore, for a highly asymmetric polymer system, asynchronicity occurs at both critical and off-critical compositions, which is responsible for the CTP and PTC transitions.

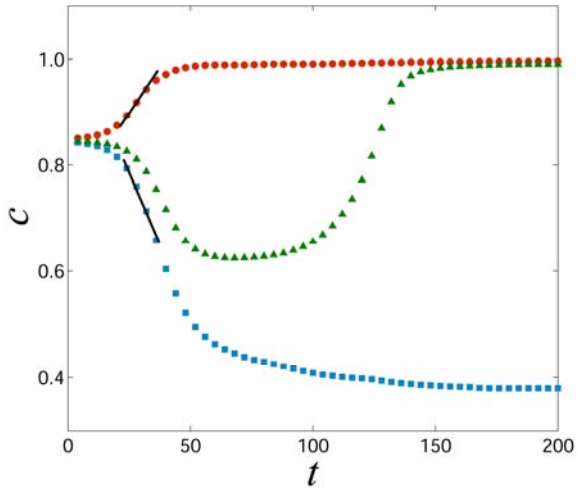

(a)

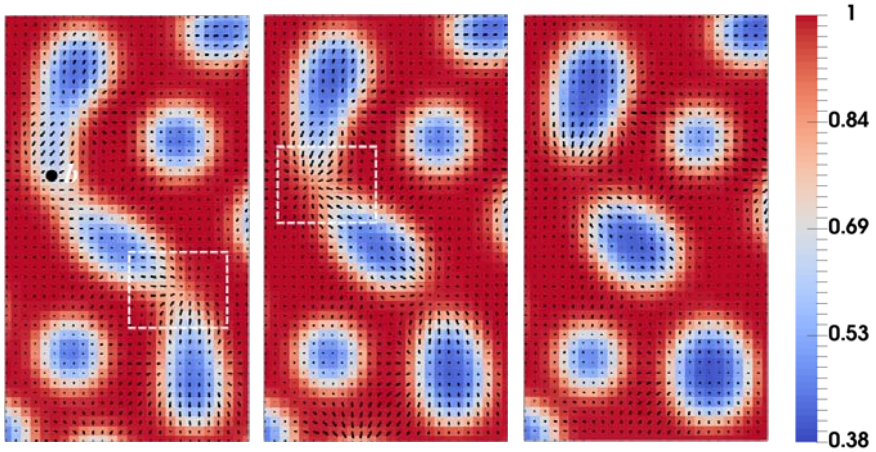

(b) (c) (d)

FIG. 6. (a) Concentration change curves of β (red) and α (blue) phases and point *b* (green) in (b) for initial composition c_0 = 0.8457; (b–d) Temporal development of local microstructure and diffusional fluxes with reduced times: t = 106, 124, and 140.

It is worth pointing out that the PTC transition in polymer systems has been mentioned in several experimental [36–41] and numerical [24,42,43] studies, where most of the systems considered have symmetrical miscibility gaps and the PTC

transition occurs at off-critical compositions. In contrast, the PTC transition observed in the current study occurs at the critical composition of a highly asymmetric system. To distinguish these two types of PTC transitions, we carry out parallel simulations for a symmetric system with $N_A = N_B = 1$ at an off-critical composition and an asymmetrical system with $N_A = 1$ and $N_B = 100$ near the critical composition to compare their MEP. For this purpose, the equilibrium concentration ranges in both cases are rescaled to [0, 1] and the initial solution compositions are chosen such that the two product phases have exactly the same volume fraction ratio at equilibrium in the two cases, i.e., $V_\beta/V_\alpha = 75{:}25$, where V_β and V_α are the equilibrium volume fraction of β and α phases, respectively. For the convenience of discussion, we call the PTC transition associated with a symmetrical miscibility gap P□TC hereafter.

The semi-logarithm plots of the structure factor $S(k_m, t)$ versus time are presented for the asymmetrical case with $c_0 = 0.8457$ in Fig. 7(a) and for the symmetric case with $c_0 = 0.65$ in Fig. 7(b). The structure factor $S(k, t)$ calculated by the circularly-averaged method [42] reaches its maximum, $S(k_m, t)$ at the wave number k_m. Note that the structure factor is frequently measured in experiments using small angle light, X-ray or neutron scattering to characterize quantitatively the kinetics during phase separation [46]. The two dashed lines in Fig. 7(a) or 7(b) are tangents to the two distinctively different parts of the $S(k_m, t)$ vs. time curves, and their intersection is defined as transition point between the early and later stages of the spinodal decomposition process [44,45]. The microstructures obtained at time moments near this transition point, e.g., $t = 50$ in the asymmetric case and $t = 215$ in symmetric cases

(marked by the red dots), are shown in the insets of Fig. 7(a) and 7(b), respectively. As one can readily see that even at the two time moments the two systems have the same $S(k_m, t)$ value of 2.3, the microstructures have distinctly different characteristics: a percolated structure with a few clusters is seen in the asymmetric case while only droplet-like structure is found in the symmetric case. Thus for the PTC transition, a percolated structure first forms during the early stage (inset in Fig. 7(a)) and then breaks up and leads to a cluster-like structure (Fig. 3(d)). However, in the P□TC transition, the cluster-like structure is already developed at the early stages (Fig. 7(b)) and stays as the cluster-like structure at the later stages. The percolated structure mentioned in the P□TC transition is actually formed at a much earlier stage marked by blue point in Fig. 7(b) than that indicated by the red dot in Fig. 7(b). Therefore, the percolation-to-cluster transition in off-critical polymer blends [36–43] is entirely different from the PTC transition found in the current study.

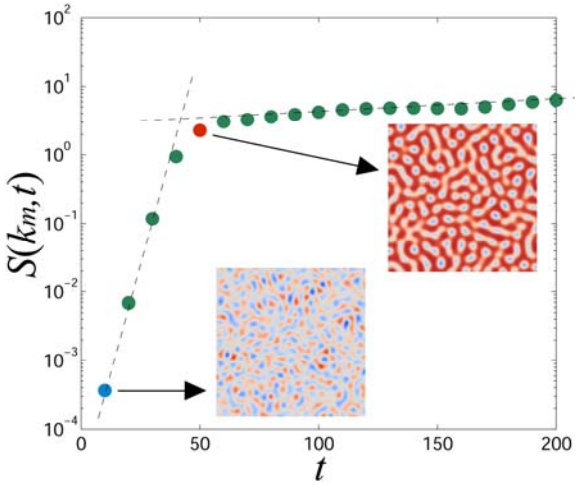

(a)

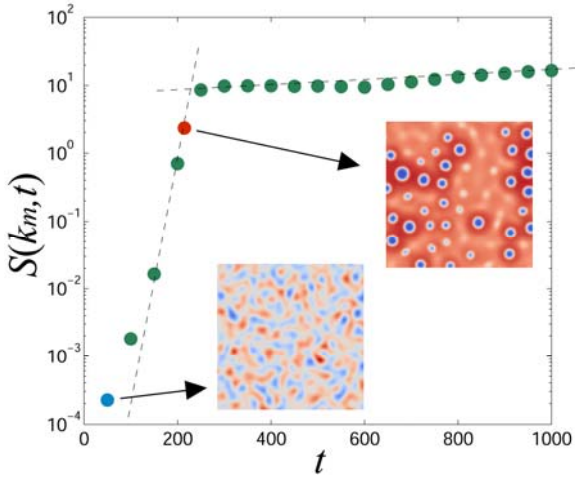

(b)

FIG. 7. Structure factor curves and patterns at the early stage: (a) for an asymmetric case with $N_A = 1$, $N_B = 100$; (b) for a symmetric case with $N_A = 1$, $N_B = 1$.

4.2. Physical origin of asynchronous growth

The above discussions suggest that the CTP and PTC transitions depend sensitively on the relative growth rate of the two product phases, e.g., v_β/v_α, where v_β and v_α are the rate of concentration variation of β and α phase domains at the early stages of spinodal decomposition and are determined in the simulations by the maximum slopes of time-evolution of concentration curves shown in Figs. 5(a) and 6(a). If v_β is significantly greater than v_α, then β cluster structure forms in a continuous α matrix. In contrast, a larger v_α will result in the formation of an α cluster structure in a continuous β matrix. On the other hand, a percolated structure can be expected when the difference between v_α and v_β is small.

To understand the growth rate difference of the solvent-rich and solvent lean domains, we focus on the thermodynamic driving force for growth because we have assumed a constant chemical mobility in this study. According to the linearized CH

equation, the application factor of the concentration wave is linearly proportional to the magnitude of the second derivative of the free energy, f'' [47]. The second derivative of the free energy of the asymmetrical polymer system considered in this study is plotted in Fig. 8. For a solution having composition c_1 (c_m, or c_2), concentration fluctuations will create solvent-lean (α phase) c_1^- (c_m^-, or c_2^-) and solvent-rich (β phase) c_1^+ (c_m^+, or c_2^+) regions. When the solution composition is far from c_m, e.g., at c_1 (or c_2), the magnitude of $f''(c_1^+)$ (or $f''(c_2^-)$) is larger than that of $f''(c_1^-)$ (or $f''(c_2^+)$) and thereby $v_\beta > v_\alpha$ (or $v_\alpha > v_\beta$). Thus, the β (or α) cluster-like structure will be obtained during the early stage. On the other hand, if the initial solution composition is located at the critical point c_m (or in the vicinity of c_m), the magnitude of $f''(c_m^-)$ is approximately same as that of $f''(c_m^+)$ and then $v_\alpha \approx v_\beta$. This will lead to an interconnected two-phase structure. The similar argument has been presented in an earlier work [21].

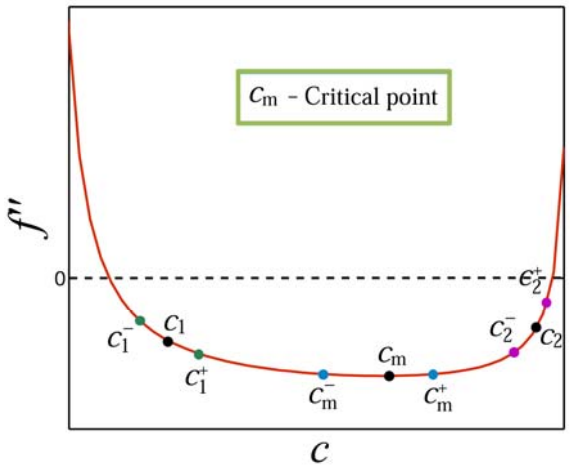

FIG. 8. Schematic drawing of second derivative of free energy density (f'') with respect to solvent composition c, where c_m represents the critical composition.

4.3. Development of MEP Map

To guide future microstructure design for polymer membranes via TIPS, below we establish an MEP map in terms of initial solution composition and aging time of phase separation in a highly asymmetric polymer system through systematic simulations. We consider microstructural characteristics at both the early and later stages of spinodal decomposition in polymer solutions having different compositions. The time-evolution of concentration, structure factor and morphological patterns obtained during the early stages are shown in Figs. 9(a) and 9(b) for point II (see Fig. 1) with c_0 = 0.6895, Figs. 9(c) and 9(d) for point IV with c_0 = 0.79, and Figs. 9(e) and 9(f) for the critical composition C with c_0 = 0.8457. Here, the structure factor curves are used to ensure that the microstructures considered are developed at the early stages. The relative growth rate v_β/v_α, measured from the slops of the concentration vs. time curves is 3.50 for c_0 = 0.6895, 1.0 for c_0 = 0.79, and 0.50 for c_0 = 0.8457, and the corresponding morphological patterns obtained are β cluster, percolated, and α cluster structures (see Figs. 9(b), 9(d), and 9(f)), which is consistent with the above analyses.

In addition, the diffusional flux field for c_0 = 0.6895 with v_β/v_α = 3.50 and for c_0 = 0.79 with v_β/v_α =1.0 are also calculated and shown in Figs. 10(a) and 10(b), which are parts of the microstructures shown in Figs. 9(b) and 9(d), respectively. The black arrows in Figs. 10(a) and 10(b) represent fluxes of the solvent. It can be seen in Fig. 10(a) that the flux gradient in the β phase domains is larger than that in the α phase domains, indicating a faster concentration evolution in the β phase domains, i.e., $v_\beta > v_\alpha$. In Fig. 10(b), the difference in flux gradient in the β and α phase domains is not

obvious, which implies that the concentration of the β phase domains approximately have the same evolution rate as that in the α phase domains, i.e., $v_\beta = v_\alpha$. Therefore, the characteristic microstructures developed during the early stages is mainly related to the relative growth rate of the two product phases, i.e., v_β/v_α.

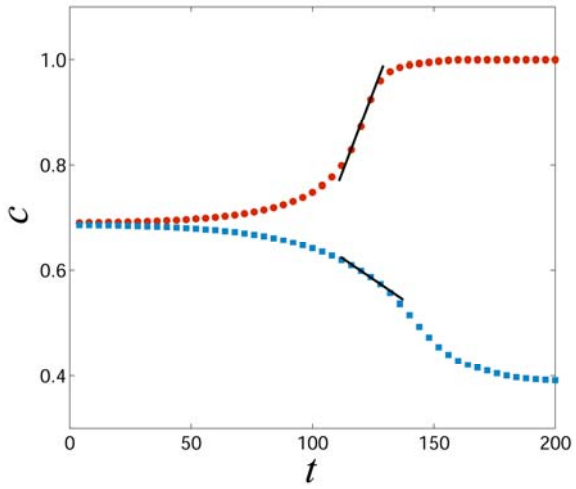

(a)

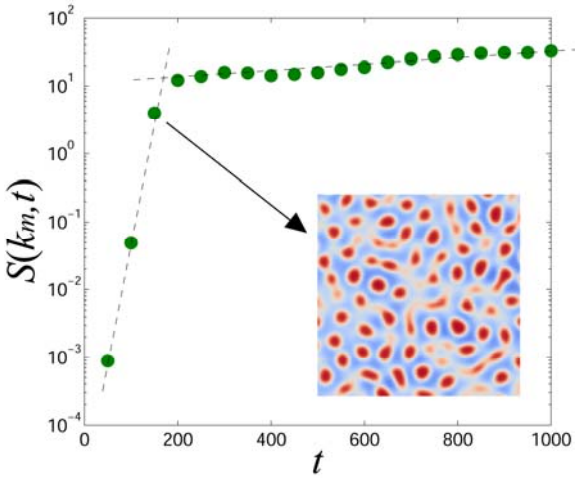

(b)

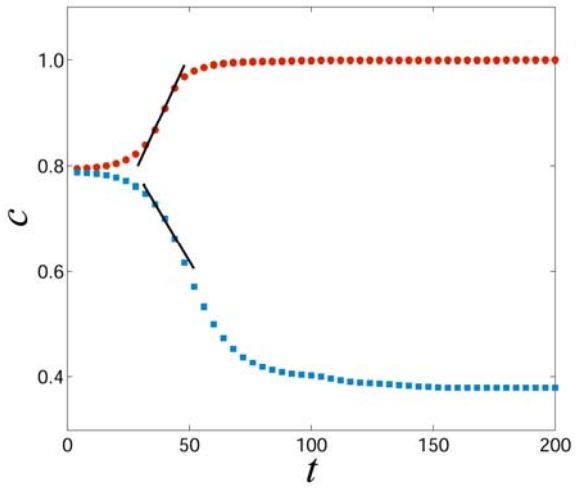
1.0
0.8
0.6
0.4
c
0
50
100
150
200
t

(c)

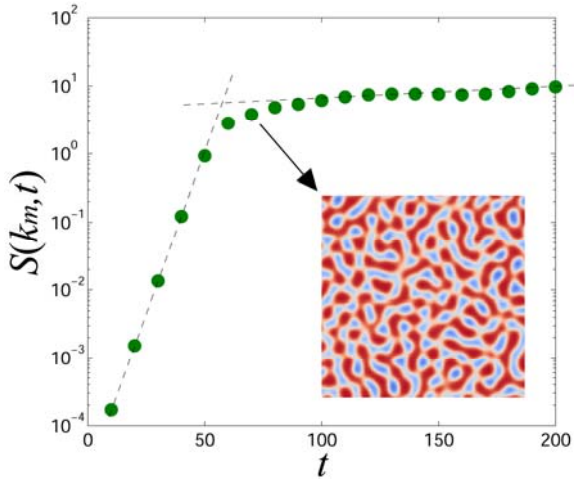
10^2
10^1
10^0
10^{-1}
10^{-2}
10^{-3}
10^{-4}
S(km,t)
0
50
100
150
200
t

(d)

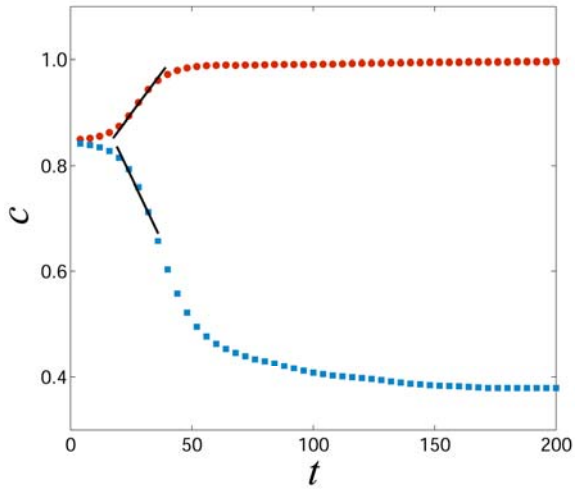
1.0
0.8
0.6
0.4
c
0
50
100
150
200
t

(e)

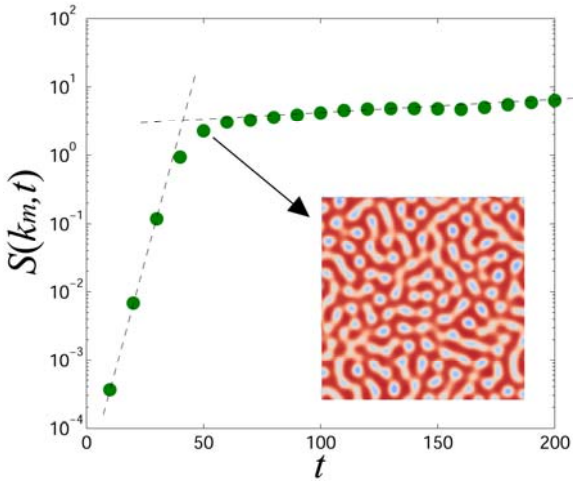

(f)

FIG. 9. Concentration variation curve, structure factor curve, and microstructure at the early stage for the initial composition: (a, b) $c_0 = 0.6895$; (c, d) $c_0 = 0.79$; (e, f) $c_0 = 0.8457$. The reduced times corresponding to the microstructures in (b), (d), and (f) are $t = 150$, $t = 70$, and $t = 50$.

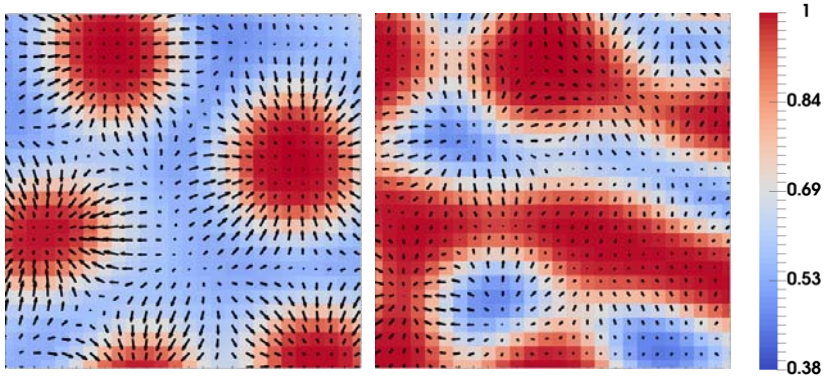

(a) (b)

FIG. 10. Locally microstructure and diffusional flux profile for initial composition and reduced time: (a) $c_0 = 0.6895$, $t = 150$; (b) $c_0 = 0.79$, $t = 70$.

In a symmetric polymer system, the microstructures developed at the later stages of spinodal decomposition can be expected by the relative volume fraction of the two product phases. However, the microstructures developed at the later stages in a highly asymmetric polymer system is determined not only by the relative volume fraction of product phases but also by the MEPs. This has been demonstrated clearly in the case with $c_0 = 0.6895$ in Fig. 2, where the relative volume fraction of the α and β phases is

50:50. Through the CTP transition, the microstructure developed in the later stages consists of discrete sausage-shaped β phase particles embedded in a continuous α phase matrix (Fig. 2(d)), other than a perfectly percolated structure. Even when the simulation time is further extended to t = 1000, the characteristics of the microstructure is still the same. Moreover, for the solution with an initial composition of c_0 = 0.8457 and V_β/V_α = 75:25, a cluster-like structure is obtained at the later stages, as shown in Fig. 3(d), which is apparently similar to the microstructure obtained from a symmetric system at an off-critical composition. However, their MEPs are quite different, being PTC in the asymmetric case and cluster-to-cluster (CTC) in the symmetric case.

Based on the above simulation results, the curve of v_β/v_α versus initial solution composition c (or the equilibrium volume fraction of the β phase, V_β) is plotted in Figs. 11(a) and the corresponding MEPs are shown in Fig. 11(b), where the markers I-V correspond to the composition points shown in Fig. 1. As shown in Fig. 11(a), the value of v_β/v_α monotonously decreases with composition and reaches unity in the vicinity of c_0 = 0.8. The MEP map in Fig. 11(b) shows four types of MEPs from the early to later stages, including cluster-to-cluster (CTC), cluster-to-percolation (CTP), percolation-to-percolation (PTP), and percolation-to-cluster (PTC). The time period for the early stages is determined according to the structure factor curve, as discussed earlier, while the start of the later stages is defined by the time when the two phases have both arrived to their equilibrium concentrations. In Fig. 11(b), the CTC pathways are located at the two ends of the MEP map and can be readily understood, since the

values of v_β/v_α and V_β/V_α for the two cases are both far from unity as seen from Fig. 11(a). The CTP and PTC transitions corresponding to composition points II and IV have been discussed earlier in above sections. In addition, the PTP transition is also observed in the map for composition point III with c_0 = 0.74, where the pattern of early stage has an approximately percolated but not perfectly percolated structure which results from the v_β/v_α of 1.79. Note that the percolated structure obtained during the late stages at composition point II with V_β/V_α = 1 is not as interconnected as that obtained for the composition point III with V_β/V_α = 1.38, which could be attributed to the asynchronous evolution of the two product phases discussed earlier.

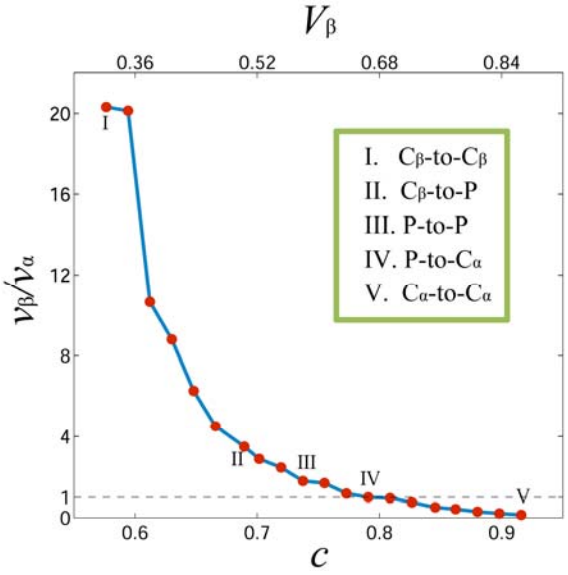

(a)

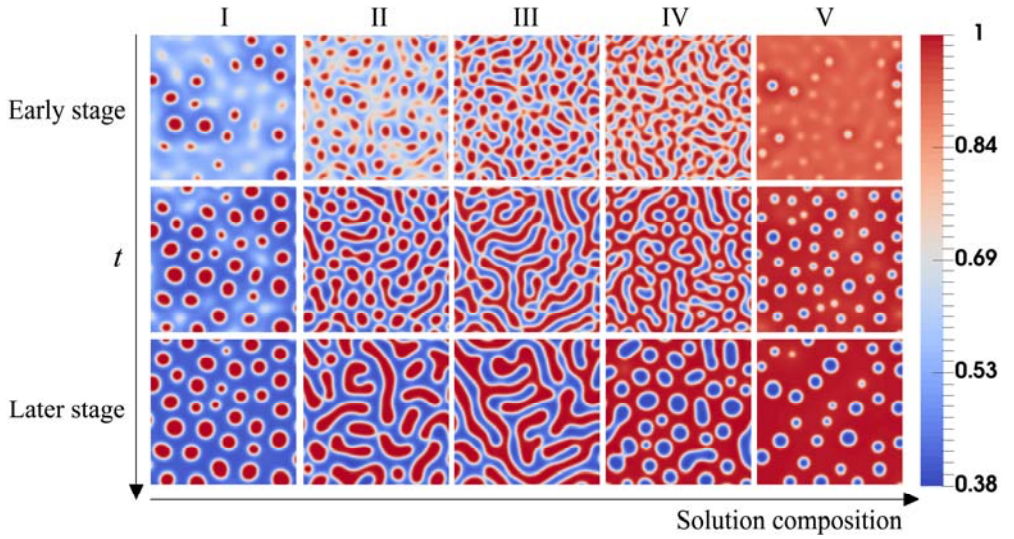

(b)

FIG. 11. (a) Relative growth rate of product phases at the early stage as a function of initial solution composition *c* (or equilibrium volume fraction of β phase); (b) the map of MEPs, including CTC, CTP, PTP, PTC transitions, where symbols C_α and C_β represent clusters of α and β phases and P is short for percolation.

Note that the above results and discussions are related to the UCST-type incompressible polymer solutions. Even though the mechanisms revealed and MEPs predicted may also shed light on the MEPs of polymer solutions with LCST as well, it should be point out that the LCST-type solutions are often considered compressible and the effect of volume change on morphology evolution should be accounted for. Thus it is highly desirable in the future to explore the MEPs of polymer solutions with LCST by adding the effect of volume change and compare them with those found for UCST-type solutions in this study.

5. SUMMARY

The microstructural evolution of a binary polymer-solvent system with a highly

asymmetric miscibility gap via thermally induced phase separation (TIPS) is investigated by computer simulations using a combination of the Flory-Huggins thermodynamics and the nonlinear Cahn-Hilliard kinetics. It is found that the morphological patterns developed at the early stages of phase separation are dictated by the relative growth rate of concentrations towards the two equilibrium product phases, while the characteristics of the morphological patterns developed during the later stages are governed by the relative volume fraction of the two product phases and the microstructural evolution pathways (MEPs). For a highly asymmetric polymer system, the two product phases asynchronously arrive at their equilibrium compositions by a hierarchical two-step process, leading to the cluster-to-percolation (CTP) and percolation-to-cluster (PTC) transitions that are not observed in symmetric polymer systems. According to the simulation results, an MEP map is established, with the initial solution composition and aging time as the input parameters. The results and analyses shown in this study can be utilized to guide future design of novel polymeric membrane synthesized by TIPS with unprecedented properties.

ACKNOWLEDGMENTS

The work was supported by the National Key Research and Development Program of China (Grant No. 2016YFB0701302), the National Natural Science Foundation of China (Grants Nos. 51671156, 51231008, and 51471125), the National Basic Research Program of China (Grants Nos. 2014CB644003, IRT13034 and 51321003) and the US Natural Science Foundation (Grant No. DMR-1410322) (YW)

and US Department of Energy (Grant No. DE-SC0001258) (YW).

REFERENCES

[1] S. Sawada, C. Ursino, F. Galiano, S. Simone, E. Drioli, and A. Figoli, *J. Membrane Sci.* **493**, 232 (2015).

[2] A. Figoli, T. Marino, S. Simone, E. di Nicolo, X. M. Li, T. He, S. Tornaghi, E. Drioli, *Green Chem.* **16**, 4034 (2014).

[3] M. Liu, Y. M. Wei, Z. L. Xu, R. Q. Guo, and L. B. Zhao. *J. Membrane Sci.* **437**, 169 (2013).

[4] Z. Y. Wang, W. Yu, and C. X. Zhou, *Polymer* **56**, 535 (2015).

[5] M. Vonka, A. Nistor, A. Rygl, M. Toulec, and J. Kosek, *Chem. Eng. J.* **284**, 357 (2016).

[6] K. Nakanishi, *J. Sol-Gel Sci. Techn.* **19**, 65 (2000).

[7] H. H. Lin, Y. H. Tang, T. Y. Liu, H. Matsuyama, and X. L. Wang, *J. Membrane Sci.* **507**, 143 (2016).

[8] N. Ghasem, M. Al-Marzouqi, and N. A. Rahim, *Sep. Purif. Technol.* **99**, 91 (2012).

[9] W. Z. Ma, S. J. Chen, J. Zhang, and X. L. Wang, *J. Macromol. Sci.* **50**, 1 (2011).

[10] P. Poesio, G. Cominardi, A. M. Lezzi, R. Mauri, and G. P. Beretta, *Phys. Rev. E* **74**, 011507 (2006).

[11] H. Matsuyama, T. Maki, M. Teramoto, and K. Asano, *J. Membrane Sci.* **204**, 323 (2002).

[12] N. T. Hassankiadeh, Z. L. Cui, J. H. Kim, D. W. Shin, A. Sanguineti, V. Arcella, Y. M. Lee, and E. Drioli, *J. Membrane Sci.* **471**, 237 (2014).

[13] X. L. Wang, H. J. Qian, L. J. Chen, Z. Y. Lu, and Z. S. Li, *J. Membrane Sci.* **311**, 251 (2008).

[14] Y. H. Tang, Y. D. He, and X. L. Wang, *J. Membrane Sci.* **437**, 40 (2013).

[15] I. Teraoka, *Polymer solutions: An introduction to physical properties* (John Wiley & Sons, New York, 2002), p. 69.

[16] J. K. Kim, K. Taki, and M. Ohshima, *Langmuir* **23**, 12397 (2007).

[17] T. Koyama and H. Tanaka, *EPL* **80**, 68002 (2007).

[18] R. Saxena and G. T. Caneba, *Polym. Eng. Sci.* **42**, 1019 (2002).

[19] Y. Mino, T. Ishigami, Y. Kagawa, and H. Matsuyama, *J. Membrane Sci.* **483**, 104 (2015).

[20] S. J. Hong and P. K. Chan, *Modelling Simul. Mater. Sci. Eng.* **18**, 025013 (2010).

[21] S. Asai, S. Majumdar, A. Gupta, K. Kargupta, and S. Ganguly, *Comp. Mater. Sci.* **47**, 193 (2009).

[22] B. F. Barton, P. D. Graham, and A. J. Mchugh, *Macromolecules* **31**, 1672 (1998).

[23] P. K. Chan and A. D. Rey, *Macromol. Theory Simul.* **4**, 873 (1995).

[24] Y. Termonia, *Macromolecules* **30**, 5367 (1997).

[25] P. D. Graham, A. J. Pervan, and A. J. Mchugh, *Macromolecules* **30**, 1651 (1997).

[26] J. W. Cahn and J. E. Hilliard, *J. Chem. Phys.* **28**, 258 (1958).

[27] V. P. Skripov and A. V. Skripov, *Usp. Fiz. Nauk* **128**, 193 (1979).

[28] P. J. Flory, *Principles of polymer chemistry* (Cornell University Press, New York, 1953), p. 495.

[29] Y. C. Li, R. P. Shi, C. P. Wang, X. J. Liu, and Y. Z. Wang, *Phys. Rev E.* **83**, 041502 (2011).

[30] J. N. Zhang, Z. L. Zhang, H. D. Zhang, and Yuliang Yang, *Phys. Rev E.* **64**, 051510 (2001).

[31] P. C. Hohenberg and B. I. Halperin, *Rev. Mod. Phys.* **49**, 435 (1977).

[32] M. Tokuyama and Y. Enomoto, *Phys. Rev E.* **47**, 1156 (1993).

[33] R. Petschek and H. Metiu, *J. Chem. Phys.* **79**, 3443 (1983).

[34] M. Okada, K. Fujimoto, and T. Nose, *Macromolecules* **28**, 1795 (1995).

[35] K. Yamanaka and T. Inoue, *Polymer* **30**, 662 (1989).

[36] J. Lauger, R. Lay, and W. Gronski, *J. Chem. Phys.* **101**, 7181 (1994).

[37] H. Takeno and T. Hashimoto, *J. Chem. Phys.* **107**, 1634 (1997).

[38] H. Takeno, M. Iwata, M. Takenaka, and T. Hashimoto, *Macromolecules* **33**, 9657 (2000).

[39] H. Takeno, E. Nakamura, and T. Hashimoto, *J. Chem. Phys.* **110**, 3612 (1999).

[40] M. Takenaka, T. Izumitani, and T. Hashimoto, *J. Chem. Phys.* **98**, 3528 (1993).

[41] I. Demyanchuk, S. A. Wieczorek, *J. Chem. Phys.* **121**, 1141 (2004).

[42] G. Brown and A. Chakrabarti, *J. Chem. Phys.* **98**, 2451 (1993).

[43] H. Chen and A. Chakrabarti, *J. Chem. Phys.* **108**, 6006 (1998).

[44] P. K. Chan and A. D. Rey, *Macromolecules* **29**, 8934 (1996).

[45] P. K. Chan and A. D. Rey, *Macromolecules* **30**, 2135 (1997).

[46] J. D. Gunton, M. San Miguel, and P. S. Sahni, *The Dynamics of First-order Phase Transitions* (Academic Press, New York, 1983), p. 267.

[47] J. E. Hilliard, *Spinodal decomposition* (American Society for Metals, Ohio, 1970), p. 497.